Eur Biophys J (2012) 41:939–947
DOI 10.1007/s00249-012-0851-3

ORIGINAL PAPER

EBSA
Biophysics in Europe

Endothelial cells undergo morphological, biomechanical, and dynamic changes in response to tumor necrosis factor-α

Kimberly M. Stroka · Janina A. Vaitkus · Helim Aranda-Espinoza

Received: 9 May 2012 / Revised: 9 August 2012 / Accepted: 17 August 2012 / Published online: 2 September 2012

Abstract The immune response triggers a complicated sequence of events, one of which is release of the cytokine tumor necrosis factor-α (TNF-α) from stromal cells, for example monocytes and macrophages. In this work we investigated the biophysical effects of TNF-α on endothelial cells (ECs), including changes in cell morphology, biomechanics, migration, and cytoskeletal dynamics. We found that TNF-α induces a wide distribution of cell area and aspect ratio, with these properties increasing on average during treatment. Interestingly, aspect ratio peaks after approximately 10 h of exposure to TNF-α, corresponding also to a peak in exerted traction forces. Meanwhile, ECs treated with TNF-α soften, and we associate this with significant increases in estimated cellular volume. In addition, our evaluation of migratory dynamics revealed an inverse correlation between cell aspect ratio and migration speed after TNF-α treatment, suggesting that cell shape may be an important functional regulator of EC migration during an inflammatory response. Finally, we addressed the basic mechanics of how the reorganization of F-actin filaments occurs during TNF-α treatment, and observed a dynamic shift of existing actin filaments. Together, our results suggest a functional link between EC morphology, biomechanics, migration, and cytoskeletal dynamics during an inflammatory response.

Keywords Cell stiffness · Cell mechanics · Immune response · Cell migration · Actin · Traction forces

Introduction

Tumor necrosis factor-alpha (TNF-α) is a cytokine produced by a variety of stromal cells, primarily monocytes and macrophages, as a result of an immune or inflammatory response. The vascular endothelium, which normally serves as a protective barrier between the blood vessel lumen and nearby tissues, undergoes a series of biological changes after binding of TNF-α, resulting in increased permeability to both macromolecules (Goldblum et al. 1989) and immune cells (Stroka and Aranda-Espinoza 2011b). One of the most prominent biological changes is the increased expression of selectins, and adhesion molecules, including intercellular adhesion molecule-1 (ICAM-1) and vascular cell adhesion molecule-1 (VCAM-1), on the surface of the endothelium (Dustin and Springer 1988). These molecules assist in the leukocyte adhesion cascade (Dustin and Springer 1988), which includes leukocyte migration along and transmigration through the vascular endothelium. At the same time, junctional molecules, for example occludin and VE-cadherin, dissociate away from the junctions, leading to reduced barrier function (Mckenzie and Ridley 2007).

There is also evidence that TNF-α affects endothelial cell (EC) morphological and biomechanical properties. For example, cells within a confluent endothelium become larger and more elongated in response to TNF-α (Stroka and Aranda-Espinoza 2011b). F-actin undergoes significant

Electronic supplementary material The online version of this article (doi:10.1007/s00249-012-0851-3) contains supplementary material, which is available to authorized users.

K. M. Stroka · J. A. Vaitkus · H. Aranda-Espinoza
Fischell Department of Bioengineering, University of Maryland, College Park, MD 20742, USA

Present Address:
K. M. Stroka (✉)
Institute for NanoBioTechnology, Johns Hopkins University, 3400 N. Charles Street, G70 New Engineering Building, Baltimore, MD 21218, USA
e-mail: kstroka@jhu.edu

reorganization and aligns along the major axis of the cell (Mckenzie and Ridley 2007; Stroka and Aranda-Espinoza 2011b; Wojciak-Stothard et al. 1998), events which are generally linked to enhanced cell contractility and stiffness. In seemingly contradictory data, cells soften after exposure to TNF-α (Kang et al. 2008; Stroka and Aranda-Espinoza 2011b). Here, we used a variety of biophysical techniques, including live cell imaging, atomic-force microscopy, traction-force microscopy, total internal reflection fluorescence microscopy, confocal microscopy, and transfection, to understand the links between EC morphology, biomechanics, and migratory dynamics after exposure of ECs to TNF-α. To simplify the system we chose to evaluate single cells, because, for example, cell–cell adhesion affects EC stiffness (Stroka and Aranda-Espinoza 2011a). These changes in EC properties are key components of the inflammatory response, yet are often overshadowed by the biological changes that occur. Together, our results suggest a functional link between EC morphology, biomechanics, migration, and cytoskeletal dynamics during an inflammatory response.

Methods

Cell culture

Human umbilical vein ECs (HUVECs) were purchased from Lifeline Cell Technology (Walkersville, MD, USA) and cultured as previously described elsewhere (Stroka and Aranda-Espinoza 2011a, b). Glass coverslips (22 × 22 mm, Fisher Scientific, Pittsburgh, PA) were coated with 0.1 mg/mL fibronectin (Sigma, St Louis, MO, USA) for 2 h at room temperature, and HUVECs (1×10^4 total; passages 2–6) were plated on to the fibronectin-coated glass coverslips. Cells were incubated at 37 °C, in 5 % CO_2 and at 55 % humidity, overnight, for approximately 16 h, and were subsequently treated with 25 ng/mL TNF-α or no treatment (control).

Cell staining

HUVECs were fixed in 0.5 % glutaraldehyde (Ted Pella, Redding, CA, USA) for 10 min and washed twice in phosphate-buffered saline (PBS). Cells were then permeabilized and blocked for nonspecific binding as described elsewhere (Stroka and Aranda-Espinoza 2011a). F-actin, nuclear DNA, and vinculin were stained as described elsewhere (Stroka and Aranda-Espinoza 2011a).

Cell transfection

Cells were transfected for GFP-actin by use of an Amaxa Nucleofector (Lonza, Walkersville, MD, USA). Primary mammalian endothelial cell solutions (Lonza) were used in combination with program A-034 on the Nucleofector, and the manufacturer's optimized procedure for HUVECs was followed. After transfection, cells were plated on to fibronectin-coated glass coverslips and left to attach overnight. Cells were then rinsed and subsequently used in fluorescence timelapse microscopy experiments.

Atomic-force microscopy

Young's moduli of live HUVECs were measured by use of an atomic-force microscope (AFM; Agilent Technologies, Santa Clara, CA, USA) as described in detail elsewhere (Stroka and Aranda-Espinoza 2011a, b). Briefly, a silicon nitride cantilever (Novascan, Ames, IA, USA) with a spherical glass SiO_2 probe of diameter 5 μm was used to obtain typical force curve measurements on live HUVECs. Twenty-five force curves were obtained for at least 10 cells for each condition (control and TNF-α), for a total of at least 250 force curves for each condition. By using custom-written Matlab (The Mathworks, Natick, MA, USA) software, data were fit to the Hertz–Sneddon model (Sneddon 1965) for a paraboloid indenter (Weisenhorn et al. 1993), as described elsewhere (Stroka and Aranda-Espinoza 2011a, b). Cells were probed at both the "cell body" (raised portion) and "periphery" (near the base of the cell body, but not at the flattened lamellipodia). Indentations were much smaller (<20 %) than the total cell height, indicating that the stiff glass substrate below the cell did not affect the force curves.

To estimate cell volume, the free and open source software Gwyddion was used. Cross-sectional plot profiles from AFM topograph images were taken across the major and minor axes of the cell (determined by eye). The plot profile was used to determine an approximate height of the cell body and periphery regions, and the lengths of the major and minor axes. The cell volume was then approximated by summing the volume of two elliptical cylindrical disks, for the flattened portion of the cell and cell body, by using the equation:

$$\pi[A_1B_1C_1 + A_2B_2(C_2 - C_1)]$$

where A_1 is half the length of the minor axis of the flattened region, B_1 is half the length of the major axis of the flattened region, C_1 is an estimate of the height of the flattened region, A_2 is half the length of the minor axis of the cell body, B_2 is half the length of the major axis of the cell body, and C_2 is an estimate of the height of the cell body (Fig. 2d).

Traction-force microscopy

Cellular traction forces were measured by use of the well-established technique of traction-force microscopy, as described in detail elsewhere (Dembo and Wang 1999;

Norman et al. 2010). Briefly, 5-kPa flexible polyacrylamide gels, composed of 8 % acrylamide and 0.07 % bisacrylamide, were embedded with 0.5-μm fluorescent marker beads and coated with 0.1 mg/mL fibronectin (Norman et al. 2010; Stroka and Aranda-Espinoza 2009). Cells were plated on to the substrates and left to adhere for ~16 h before addition of TNF-α. Phase-contrast and fluorescence images of the spread cells and embedded beads were captured, and trypsin–EDTA was added to remove the cells. An image of the relaxed marker beads was captured. On the basis of the mechanical properties of the gel and the displacements of the marker beads, the cellular traction forces were computed by use of the technique described by Dembo and Wang (1999). The overall force exerted by the cell, $|\bar{F}|$, is an integral of the traction field magnitude over the area of the cell, $|\bar{F}| = \iint \sqrt{T_x^2(x,y) + T_y^2(x,y)}\mathrm{d}x\mathrm{d}y$ where $\bar{T}(x,y) = [T_x(x,y), T_{y(x,y)}]$ is the continuous field of traction vectors defined at the spatial position (x, y) within the cell, as described elsewhere (Smith et al. 2007).

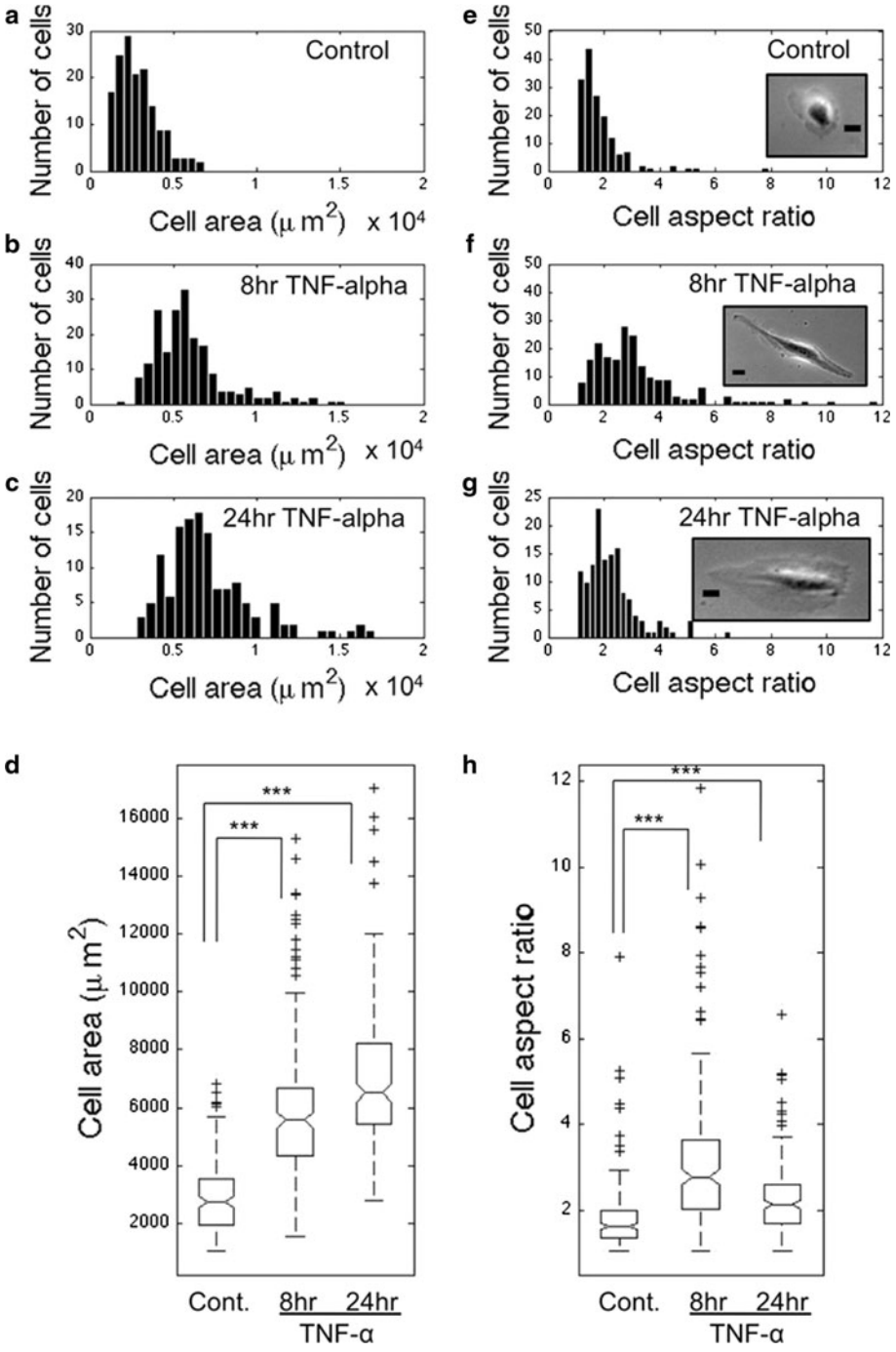

Fig. 1 TNF-α induces changes in endothelial cell (EC) morphology. Shown are histograms of cellular area for **a** control, **b** 8-h TNF-α-treated, and **c** 24-h TNF-α-treated ECs. **d** Box and whisker plots indicate that average cellular area increases with TNF-α treatment. Also shown are histograms of cellular aspect ratio, calculated by dividing the length of the major axis by the minor axis, for **e** control, **f** 8-h TNF-α-treated, and **g** 24-h TNF-α-treated ECs. *Insets* in **e**, **f**, and **g** are representative images of cells for each condition. *Scale bars* for all *insets* are 20 μm. **h** Box and whisker plots indicate that average cellular aspect ratio increases with TNF-α treatment, with aspect ratios at 8 h being significantly higher than those at 24 h. *** Indicates $P < 0.001$ using a Student's t test

Phase and fluorescence microscopy

Phase-contrast image timelapse sequences were taken in HUVEC culture media at 37 °C, in 5 % CO_2, and at 55 % humidity, by using an Olympus IX71 (Olympus, Center Valley, PA, USA) inverted microscope and a 10×/0.3 NA Ph1 objective. Images were captured by use of a QImaging Retiga-SRV charge-coupled device (CCD) digital camera (QImaging Corporation, Surrey, British Columbia, Canada) and IPLab software as described elsewhere (Stroka and Aranda-Espinoza 2011b). Fluorescence images of GFP-actin-transfected cells were taken in HUVEC culture media at 37 °C, in 5 % CO_2, and at 55 % humidity, by using an Olympus IX81 inverted microscope and a 60×/1.42 NA oil objective. Images were captured by use of a QImaging Rolera-MGi CCD digital camera (QImaging Corporation) and Slidebook software. Confocal images of cells stained for tubulin and F-actin were taken under room conditions by use of an Olympus IX81 scanning disk confocal microscope and a 60×/1.42 NA oil objective. Images were captured by using a Hammamatsu ORCA-ET CCD camera (Leeds Precision Instruments, Minneapolis, MN, USA) with Slidebook software. Cell morphology (area and aspect ratio) were measured using ImageJ (NIH, Bethesda, MD, USA) as described elsewhere (Stroka and Aranda-Espinoza 2009, 2011a). Cell speeds were calculated for each frame of the movie by dividing the cell's displacement by the time step (20 min). Then, a moving average of the 5 previous timepoints was plotted (as in Figs. 3, 4) to smooth the data. Total internal reflection fluorescence (TIRF) microscopy was completed on cells immunostained for vinculin, as described in detail elsewhere (Stroka and Aranda-Espinoza 2011a). Focal adhesion (FA) size and density were measured by using Image J for the TIRF microscopy images (Stroka and Aranda-Espinoza 2011a).

Results

TNF-α induces changes in cell morphology

HUVECs were plated on to glass coverslips and left to spread for approximately 16 h, although maximum spreading occurred after only 1 h. Subsequently, phase-contrast images were taken, and the cells were then treated with a physiological concentration of TNF-α (25 ng/mL) in culture medium. Phase-contrast images were taken 8 and 24 h after treatment. Before TNF-α treatment, a distribution of areas was observed for HUVECs (Fig. 1a); addition of TNF-α resulted in a shift of this distribution to the right after 8 h of treatment (Fig. 1b), and further to the right after 24 h of treatment (Fig. 1c). Importantly, at 24 h, untreated (control) cell area was no different from cell area at 0 h. Although increases in cell area and aspect ratio have previously been reported for TNF-α (Mckenzie and Ridley 2007; Stroka and Aranda-Espinoza 2011b; Yang et al. 2005), here we also noted that the width of the distribution of areas became noticeably wider

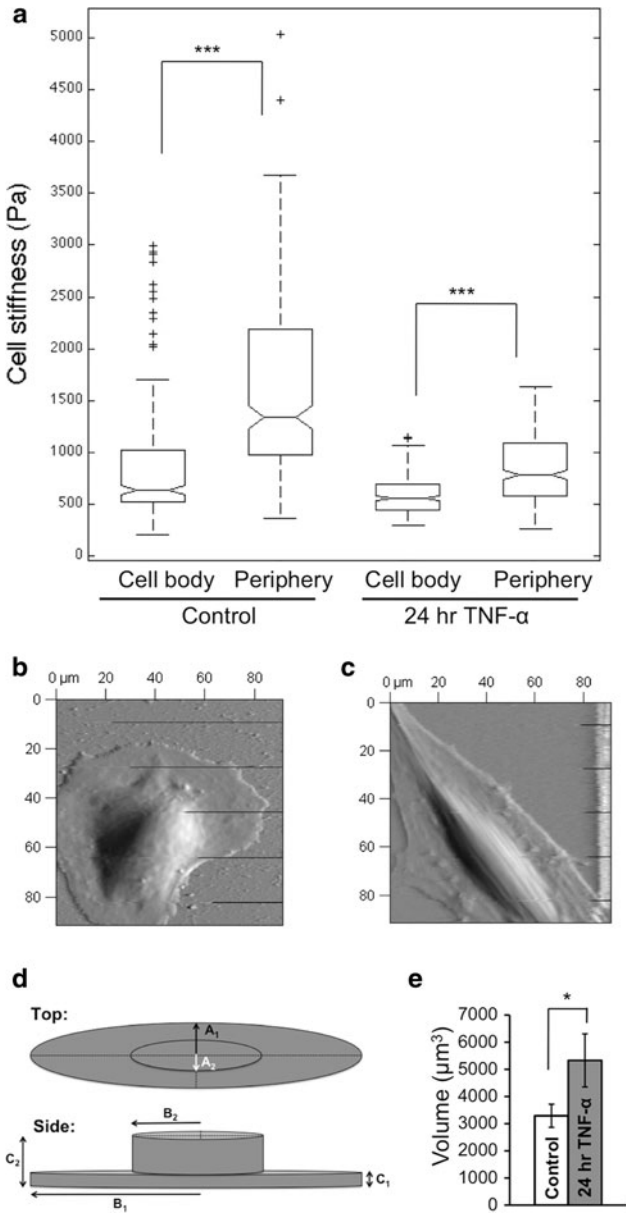

Fig. 2 TNF-α induces changes in EC mechanical properties. **a** Box and whisker plot indicates EC stiffness decreases with 24-h TNF-α treatment, both at the cell body and periphery regions, as measured by atomic-force microscopy (AFM). *** Indicates $P < 0.001$ using a Student's *t* test. AFM deflection images of **b** control and **c** 24-h TNF-α-treated ECs reveal the drastic change in morphology of most cells that occurs upon TNF-α exposure. AFM images are 90 μm by 90 μm. **d** By using AFM topographic information, cellular volume was estimated by summing the volume of two ellipsoids, for the flattened portion of the cell and cell body, by using the equation and procedure outlined in the "Methods" section. *Top* and *side views* of the relevant dimensions are shown. **f** Estimates of cellular volume for control and 24-h TNF-α-treated ECs. * Indicates $P < 0.05$ using a Student's *t* test

after the 24-h treatment (Fig. 1c). The increase in cell area throughout the treatment was also apparent from the average areas of untreated cells compared with cells 8 and 24 h after addition of TNF-α ($P < 0.001$) (Fig. 1d).

HUVECs also underwent a change in aspect ratio as a result of TNF-α treatment. In comparison with the distribution of aspect ratios before treatment (Fig. 1e), 8 h after addition of TNF-α, HUVECs were more elongated, as evidenced by the shift in the aspect ratio distribution peak to the right (Fig. 1f). At 24 h, the distribution shifted back to the left, although the distribution peak was still at a significantly larger aspect ratio than for control cells (Fig. 1g). The degree of elongation varied from the box-like morphology of untreated cells (Fig. 1e, inset), to an extremely extended morphology (Fig. 1f, inset), with aspect ratio approximately 10. The average aspect ratios of control cells versus cells at 8 and 24 h after addition of TNF-α followed the trend of the distribution peaks and were statistically different from each other ($P < 0.001$) (Fig. 1h).

TNF-α induces changes in cell biomechanical properties

By using AFM, we measured the stiffness (Young's modulus) of HUVECs, both for the periphery and cell body regions. As reported elsewhere, the cell body of control cells was softer than the periphery region (Stroka and Aranda-Espinoza 2011a) (Fig. 2a). The same trend was measured for cells after 24-h exposure to TNF-α (Fig. 2a). In addition, cells treated with TNF-α were softer than control cells at both the cell body and periphery regions ($P < 0.001$) (Fig. 2a). AFM deflection images of control (Fig. 2b) and TNF-α-treated (Fig. 2c) cells indicate the drastic changes in the morphology of most cells that occurred after exposure to TNF-α. We also estimated cellular volume from the AFM topographic images. Average estimated cell volume was larger for cells treated with TNF-α for 24 h, in comparison with untreated control cells ($P < 0.05$) (Fig. 2e).

Using traction-force microscopy, we also measured traction forces generated by HUVECs during TNF-α treatment. Average traction forces increased approximately twofold after 24 h of exposure to TNF-α (Fig. 3a). Interestingly, traction force generation was dynamic, reaching a peak in magnitude approximately 10 h after addition of TNF-α (Fig. 3b). Meanwhile, TNF-α treatment did not affect FA size ($P > 0.05$), but reduced FA density ($P < 0.001$) and caused the FAs to elongate and align along the major length of the cell (Fig. 3c–f), an effect that might contribute to the increase in traction forces exerted by the cells.

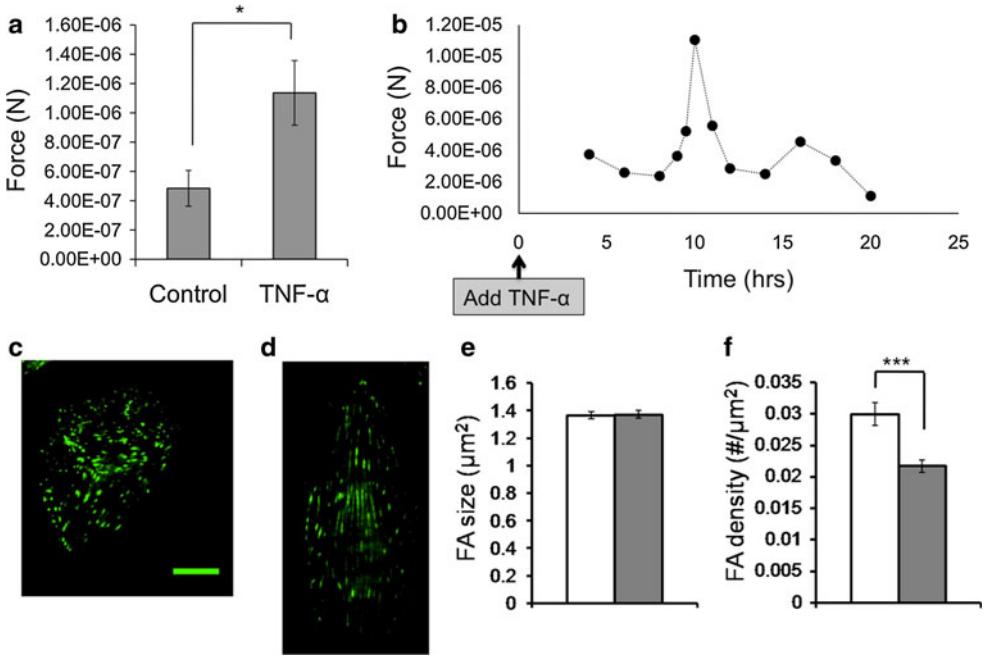

Fig. 3 TNF-α exposure increases traction force generation in ECs and reduces focal adhesion density. **a** Average traction force exerted by control and 24-h TNF-α-activated ECs. *Error bars* indicate average of 7 and 10 experiments for control and TNF-α-activated ECs, respectively. * Indicates $P < 0.05$ using a Student's t test. **b** Change in traction force generation for a representative cell compared with untreated condition, over the course of TNF-α treatment. TNF-α was added at $T = 0$ as indicated. Also shown are total internal reflection fluorescence (TIRF) microscopy images of vinculin-stained **c** control ECs and **d** ECs treated with TNF-α for 24 h. In **c**, the *scale bar* is 20 μm and also applies to **d**. Focal adhesion size (**e**) and density (**f**) were quantified by use of image analysis. *** Indicates $P < 0.001$ using a Student's t test. *Bars* are mean ± SEM

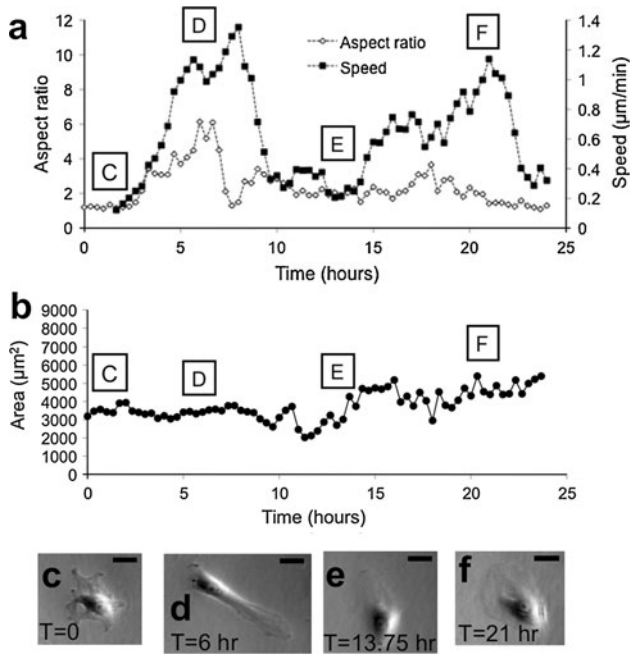

Fig. 4 Cell speed is not necessarily correlated with aspect ratio for migrating control ECs. **a** Cell aspect ratio (primary axis) and speed (secondary axis) are plotted on the same axis for a representative migrating control cell. **b** Cell area is plotted as a function of time. In **a**, **b**, time = 0 corresponds to ~16 h after plating cells. In **a**, *letters C–F* correspond to timepoints relevant to the images shown in **c–f**, respectively. *Scale bar* is 20 μm for all images

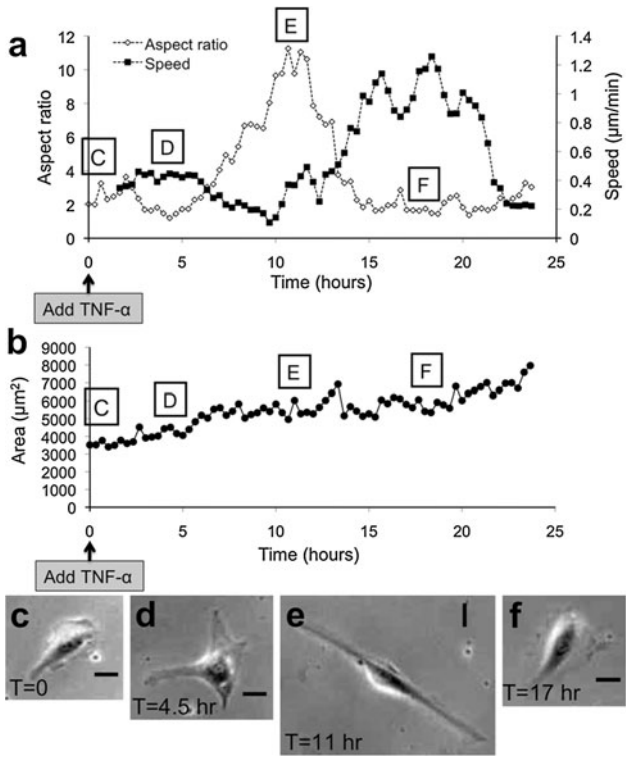

Fig. 5 Cell speed is inversely correlated with aspect ratio for TNF-α-activated ECs. **a** Cell aspect ratio (primary axis) and speed (secondary axis) are plotted on the same axis for a representative migrating TNF-α-activated cell. **b** Cell area is plotted as a function of time. In **a**, **b**, time = 0 corresponds to ~16 h after plating cells, which is the time when TNF-α was added to the cell media. In **a**, *letters C–F* correspond to timepoints relevant to the images shown in **c–f**, respectively. *Scale bar* is 20 μm for all images

TNF-α induces an inverse correlation between cell aspect ratio and migration speed

By using phase contrast timelapse microscopy we also evaluated the migratory behavior of HUVECs in response to TNF-α. For untreated control cells, aspect ratio and migration speed were not necessarily correlated. For example, in the representative cell shown in Fig. 4a, as the time reached point D on the plot, there was first a peak in speed that correlated with a peak in aspect ratio; however, the aspect ratio then decreased as the migration speed continued to increase. There was an additional peak in speed at point F, but this was not correlated with any changes in aspect ratio. Over the 24-h period (of no treatment), the area of the control cell fluctuated and finally increased slightly. However, on average, control cells were not larger after 24 h. The aspect ratio data at points C, D, E, and F on Fig. 4a correspond to the phase-contrast images shown in Fig. 4c, d, e, and f, respectively.

In agreement with the average aspect-ratio trends at 8 and 24 h after addition of TNF-α (Fig. 1h), most cells tracked individually underwent a peak in aspect ratio within the first 15 h of TNF-α treatment, as for the representative cell shown in Fig. 5a. Interestingly, for TNF-α-treated cells, aspect ratio was usually inversely correlated with cell migration speed (Fig. 5a). For example, migration speed fell to the lowest value just before the aspect ratio peaked near point E in Fig. 5a. Later, at point F, aspect ratio decreased rapidly as migration speed increased to a peak value. In addition, cell area increased steadily over 24 h of TNF-α treatment (Fig. 5b), which is in agreement with the average cell areas at 8 and 24 h after addition of TNF-α (Fig. 1d). The aspect ratio data at points C, D, E, and F on Fig. 5a correspond to the phase-contrast images shown in Fig. 5c, d, e, and f, respectively. This same cell is featured in Movie 1 in the Electronic Supplementary Material.

TNF-α induces alignment of actin filaments along the major axis of cells

To evaluate the effects of TNF-α on the HUVEC cytoskeletal architecture, we stained for F-actin and captured confocal images of the cells. In control ECs, mature stress fibers formed and were arranged in parallel groups along the basal surface of the cells (Fig. 6). Activation of the cells with TNF-α induced significant changes in the F-actin

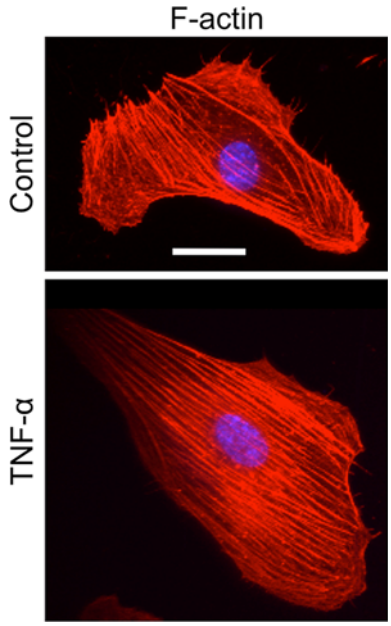

Fig. 6 TNF-α exposure induces F-actin alignment along the cell major axis. ECs stained for F-actin (*red*) or DNA (*blue*) are shown for representative control and 24-h TNF-α-treated cells. *Scale bar* is 20 μm and applies to both images

organization of ECs. After 24-h treatment with TNF-α, most cells' F-actin was arranged parallel to the major (long) axis of the cell (Fig. 6).

TNF-α induces dynamic actin rearrangement

In addition to a static assessment of the effects of TNF-α on cytoskeletal architecture, we also evaluated how the transition occurred dynamically. Specifically, we aimed to address the question of whether the F-actin reorganization involved depolymerization and repolymerization of actin, or whether it was simply a shift of existing actin fibers. Thus, we transfected HUVECs for GFP-actin and captured fluorescence images over the entire 24-h period of TNF-α treatment. The timelapse sequence in Fig. 7, (also see Movie 2 in Electronic Supplementary Material), indicates the dynamic shift of F-actin inward towards the nucleus as the polymers aligned in parallel along the major axis of the cell.

Discussion

The immune response triggers a complicated sequence of events, one of which is release of the cytokine TNF-α from stromal cells, for example monocytes and macrophages. Although the biological effects of TNF-α have been studied, here we focus on less-studied aspects of the inflammatory response, including EC morphology, biomechanics, migration, and cytoskeletal dynamics. These properties are important because, for example, neutrophils are mechanosensitive (Oakes et al. 2009; Stroka and Aranda-Espinoza 2009), and the biophysical properties of ECs are beginning to be understood as key regulators of the inflammatory response (Stroka and Aranda-Espinoza 2010).

One of the most striking results of our work is the relationship between cell aspect ratio, traction force, and migration speed during exposure to TNF-α. We report, for the first time, an interesting trend in which aspect ratio peaks at approximately $T = 8$–10 h, and then drops off as time approaches 24 h (Fig. 1e–h). This morphology behavior is also related to the migratory dynamics of the cell, because cell speed and aspect ratio are inversely correlated in TNF-α-treated cells (Fig. 5), but not in control cells (Fig. 4). Further, a peak in traction force after approximately 10 h of treatment (Fig. 3b) is nearly concurrent with the maximum aspect ratio. We suggest that this relationship between aspect ratio, migration, and traction force arises because a high cellular aspect ratio does not promote efficient migration, and thus an elongated cell must first detach at the rear in order to migrate forward. Detachment requires contractile forces, which could explain the peak in traction forces that we observe after approximately 10 h of TNF-α treatment (Fig. 3b).

We also suggest that these changes in cell shape, biomechanics, and migration are related to cytoskeletal dynamics. The shift of F-actin over the first several hours of TNF-α treatment (Fig. 7) indicates that changes in aspect ratio involve, or are even caused by, alterations in the cell's cytoskeleton. Thus, the changes in aspect ratio induced by TNF-α exposure are likely to be explained by F-actin arrangement.

While decreases in cell stiffness after 24 h of TNF-α exposure (Fig. 2) are consistent with previous reports (Kang et al. 2008; Stroka and Aranda-Espinoza 2011b), these results are somewhat counterintuitive with regard to the morphological changes we observed. Specifically, increased F-actin (Fig. 6) and traction forces (Fig. 3b) have been associated with increases in cell stiffness (Wang et al. 2002). In addition, TNF-α exposure has been found to initiate the Rho, ROCK, and myosin light chain kinase (MLCK) signaling pathways which are associated with cell contraction (Mckenzie and Ridley 2007). However, an important consideration here is that force measurements made by AFM utilize an indentation that is very small compared with the total height of the cell, and thus the Young's modulus measurements that we report are not necessarily reflective of the basal surface of the cell, where the stress fibers are located. Rather, our measurements are reflective of cell cytoplasmic or cortical actin stiffness. Thus, the significant increase in estimated cellular volume with TNF-α treatment (Fig. 2e) could explain the decrease

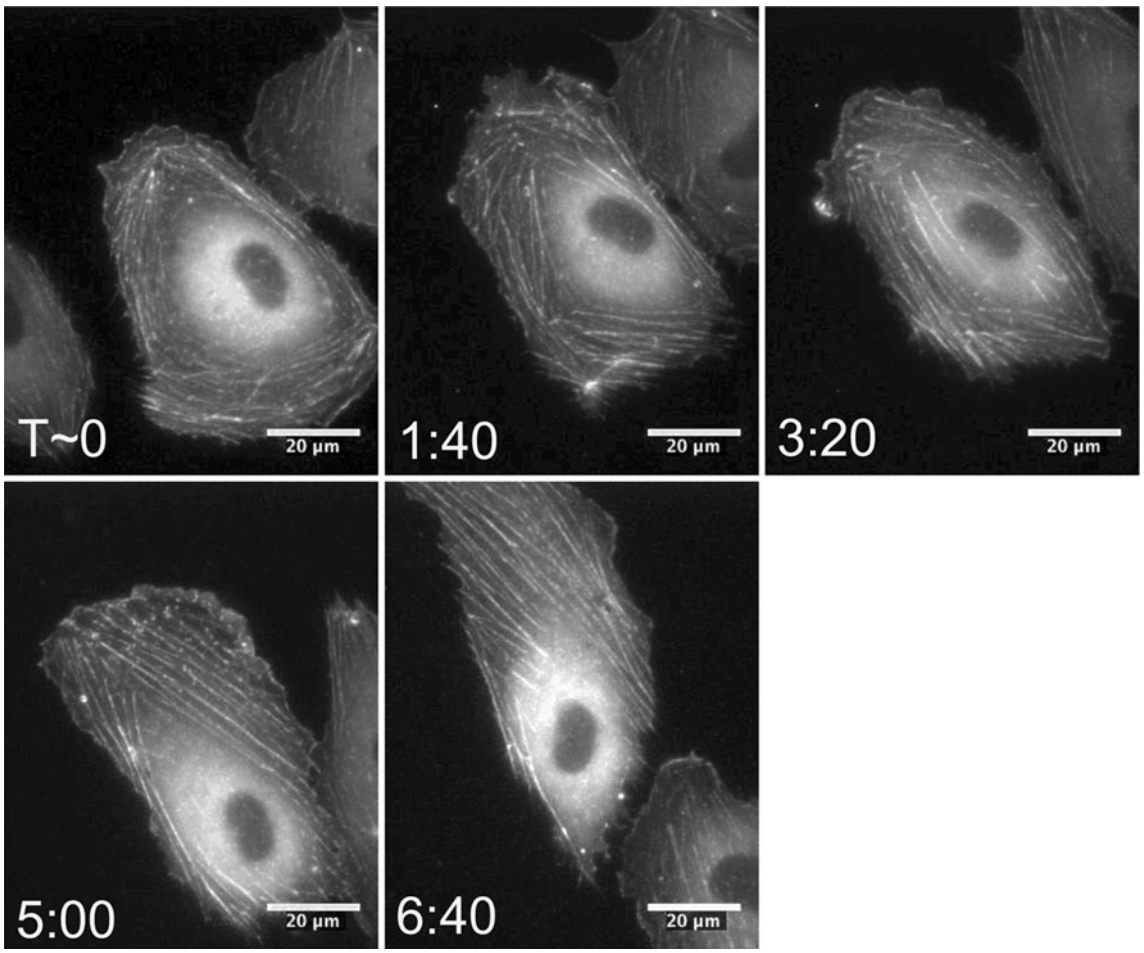

Fig. 7 TNF-α-induced changes in the F-actin cytoskeleton involve a dynamic shift of existing actin filaments. ECs were transfected with GFP-actin and fluorescence images were captured after addition of TNF-α. A time sequence for a representative cell is shown. *Scale bar* is 20 μm and applies to all images. *T* indicates the time (in hours:minutes format) after which TNF-α was added to the cell media

in cell stiffness, despite changes in F-actin and traction forces that might suggest opposite effects on stiffness. To the best of our knowledge, we are the first to report an increase in EC volume after 24 h of TNF-α treatment, although TNF-α has previously been implicated in regulation of ion channels, which play a significant role in cell volume regulation. It has been reported that in smooth muscle cells TNF-α treatment activates swelling-activated chloride channels (Matsuda et al. 2010) and also enhances the peak and plateau levels of intracellular Ca^{2+} levels in response to acetylcholine and bradykinin (White et al. 2006). Further, an increase in stress fiber formation is a key characteristic of TNF-α treatment (Mckenzie and Ridley 2007); we expect that this event is accompanied by an influx of water and ions, thus increasing cell volume. Therefore, the overall increase in cellular volume that we measure by use of AFM is likely to be caused by TNF-α-induced activation of volume-regulating ion channels.

Conclusions

Here, we demonstrated the relationships between cellular morphology, biomechanics, migration, and cytoskeletal dynamics during an inflammatory response. Previously, much attention has focused on the biological signaling which results from cytokine exposure, though little work has focused on the biomechanics and dynamics of ECs in response to TNF-α. These biophysical properties of the vascular endothelium are key aspects of the immune response and are therefore likely to affect the efficiency of the leukocyte adhesion cascade.

Acknowledgments We thank Dr Micah Dembo for providing the Fortran code to analyze traction force data and for engaging in useful discussions about traction forces. This work was supported by a National Institutes of Health National Research Service Award F31NS068028 (K.M.S.) and NSF Award CMMI-0643783 (H.A.E.). The content is solely the responsibility of the authors and does not

necessarily represent the official views of the National Institute of Neurological Disorders and Stroke or the National Institutes of Health.

References

Dembo M, Wang YL (1999) Stresses at the cell-to-substrate interface during locomotion of fibroblasts. Biophys J 76:2307–2316

Dustin ML, Springer TA (1988) Lymphocyte function-associated antigen-1 (LFA-1) interaction with intercellular adhesion molecule-1 (ICAM-1) is one of at least three mechanisms for lymphocyte adhesion to cultured endothelial cells. J Cell Biol 107:321–331

Goldblum SE, Hennig B, Jay M, Yoneda K, McClain CJ (1989) Tumor necrosis factor alpha-induced pulmonary vascular endothelial injury. Infect Immun 57:1218–1226

Kang I, Panneerselvam D, Panoskaltsis VP, Eppell SJ, Marchant RE, Doerschuk CM (2008) Changes in the hyperelastic properties of endothelial cells induced by tumor necrosis factor-alpha. Biophys J 94:3273–3285

Matsuda JJ, Filali MS, Moreland JG, Miller FJ, Lamb FS (2010) Activation of swelling-activated chloride current by tumor necrosis factor-alpha requires ClC-3-dependent endosomal reactive oxygen production. J Biol Chem 285:22862–22871

Mckenzie JAG, Ridley AJ (2007) Roles of Rho/ROCK and MLCK in TNF-alpha-induced changes in endothelial morphology and permeability. J Cell Physiol 213:221–228

Norman LL, Oetama RJ, Dembo M, Byfield F, Hammer DA, Levitan I, Aranda-Espinoza H (2010) Modification of cellular cholesterol content affects traction force, adhesion and cell spreading. Cell Mol Bioeng 3:151–162

Oakes PW, Patel DC, Morin NA, Zitterbart DP, Fabry B, Reichner JS, Tang JX (2009) Neutrophil morphology and migration are affected by substrate elasticity. Blood 114:1387–1395

Smith LA, Aranda-Espinoza H, Haun JB, Dembo M, Hammer DA (2007) Neutrophil traction stresses are concentrated in the uropod during migration. Biophys J 92:L58–L60

Sneddon IN (1965) The relation between load and penetration in the axisymmetric Boussinesq problem for a punch of arbitrary profile. Int J Eng Sci 3:47–57

Stroka KM, Aranda-Espinoza H (2009) Neutrophils display biphasic relationship between migration and substrate stiffness. Cell Motil Cytoskeleton 66:328–341

Stroka KM, Aranda-Espinoza H (2010) A biophysical view of the interplay between mechanical forces and signaling pathways during transendothelial cell migration. FEBS J 277:1145–1158

Stroka KM, Aranda-Espinoza H (2011a) Effects of morphology vs. cell–cell interactions on endothelial cell stiffness. Cell Mol Bioeng 4:9–27

Stroka KM, Aranda-Espinoza H (2011b) Endothelial cell substrate stiffness influences neutrophil transmigration via myosin light chain kinase-dependent cell contraction. Blood 118:1632–1640

Wang N, Tolic-Norrelykke IM, Chen J, Mijailovich SM, Butler JP, Fredberg JJ, Stamenovic D (2002) Cell prestress. I. Stiffness and prestress are closely associated in adherent contractile cells. Am J Physiol Cell Physiol 282:C606–C616

Weisenhorn AL, Khorsandit M, Kasast S, Gotzost V, Butt H-J (1993) Deformation and height anomaly of soft surfaces studied with an AFM. Nanotechnology 4:106–113

White TA, Xue AL, Chini EN, Thompson M, Sieck GC, Wylam ME (2006) Role of transient receptor potential C3 in TNF-alpha-enhanced calcium influx in human airway myocytes. Am J Resp Cell Mol 35:243–251

Wojciak-Stothard B, Entwistle A, Garg R, Ridley AJ (1998) Regulation of TNF-alpha-induced reorganization of the actin cytoskeleton and cell–cell junctions by Rho, Rac, and Cdc42 in human endothelial cells. J Cell Physiol 176:150–165

Yang L, Froio RM, Sciuto TE, Dvorak AM, Alon R, Luscinskas FW (2005) ICAM-1 regulates neutrophil adhesion and transcellular migration of TNF-alpha-activated vascular endothelium under flow. Blood 106:584–592